Materials Research Letters

ISSN: (Print) 2166-3831 (Online) Journal homepage: http://www.tandfonline.com/loi/tmrl20

Tiny MoO_3 nanocrystals self-assembled on folded molybdenum disulfide nanosheets via a hydrothermal method for supercapacitor

S. V. Prabhakar Vattikuti, P. C. Nagajyothi, Police Anil Kumar Reddy, Mandari Kotesh Kumar, Jaesool Shim & Chan Byon

To cite this article: S. V. Prabhakar Vattikuti, P. C. Nagajyothi, Police Anil Kumar Reddy, Mandari Kotesh Kumar, Jaesool Shim & Chan Byon (2018) Tiny MoO_3 nanocrystals self-assembled on folded molybdenum disulfide nanosheets via a hydrothermal method for supercapacitor, Materials Research Letters, 6:8, 432-441, DOI: 10.1080/21663831.2018.1477848

To link to this article: https://doi.org/10.1080/21663831.2018.1477848

MATER. RES. LETT.
2018, VOL. 6, NO. 8, 432–441
https://doi.org/10.1080/21663831.2018.1477848

MATERIALS RESEARCH LETTERS
Taylor & Francis
Taylor & Francis Group

ORIGINAL REPORT

Tiny MoO_3 nanocrystals self-assembled on folded molybdenum disulfide nanosheets via a hydrothermal method for supercapacitor

S. V. Prabhakar Vattikuti [a*], P. C. Nagajyothi[a*], Police Anil Kumar Reddy[b], Mandari Kotesh Kumar[a], Jaesool Shim[a] and Chan Byon[b]

[a]School of Mechanical Engineering, Yeungnam University, Gyeongsan, South Korea; [b]School of Mechanical and Nuclear Engineering, Ulsan National Institute of Science and Technology (UNIST), Ulsan, Republic of Korea

ABSTRACT

Coupling of two active semiconductors can easily lead to a deterioration of their intrinsic properties. In this work, tiny MoO_3 nanocrystals were deposited on 3D MoS_2 frameworks via a hydrothermal reaction, with heterostructures forming by oxygen-bonding interactions at their interface. When tested as a supercapacitor electrode, the MoS_2/MoO_3 heterostructure exhibited a high specific capacitance of 287.7 F g^{-1} at a current density of 1 A g^{-1}, and a remarkable cycling stability after 1000 cycles at 1 A g^{-1} in an aqueous solution compared to pristine MoS_2. The results thus reveal the superior properties of the MoS_2/MoO_3 heterostructure for supercapacitor electrode.

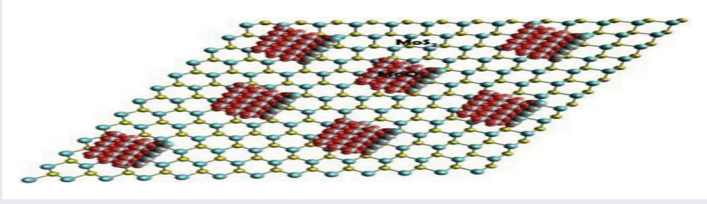

IMPACT STATEMENT

We successfully synthesized tiny MoO_3 nanocrystals deposited on 3D MoS_2 frameworks via a self-assembly. The MoS_2/MoO_3 heterostructure exhibited a high specific capacitance and cycling stability compared to pristine MoS_2.

ARTICLE HISTORY
Received 2 February 2018

KEYWORDS
Heterojunction; layered materials; supercapacitor; MoS_2

1. Introduction

Supercapacitors that can realize the conversion of chemical energy are currently predominantly used in power supplies with an extensive range of applications. Studies on the design and development of supercapacitor electrode materials have shown their great promise in providing significant improvements in practical applications. To meet the requirements of energy storage applications based on the electrochemical performance of electrodes, a vigorous pursuit of active materials with long-term cyclic stability is necessary [1–3]. Because exposed edge sites show excellent electrochemical performance, the use of two-dimensional (2D) layered MoS_2 as an electrode material has recently gained significant attention. Numerous studies have demonstrated that MoS_2 materials on various structures exhibit superior electrochemical performance for supercapacitor applications [4,5]. The structure of MoS_2 is analogous to graphite in which one layer of Mo atoms is sandwiched by two layers of S atoms forming a three-atom layer. These layers are stacked together by weak van der Waal forces of attractions. The interlayer spacings of these stacked layers play an important role in determining the thermal and electrical conductivities of the MoS_2. The improved spacings in between the MoS_2 sheets significantly reduce the energy barrier required for the intercalation and transportation of ions (enhanced redox reactions) and thus improve the supercapacitor performance. Hence, many researchers across the globe are working on improving the interlayer spacings of the MoS_2 layers

CONTACT S. V. Prabhakar Vattikuti vsvprabu@gmail.com; Jaesool Shim jshim@ynu.ac.kr School of Mechanical Engineering, Yeungnam University, 214-1 Dae-dong Gyeongsan-si, Gyeongsangbuk-do, 712-749 Gyeongsan, South Korea
*These authors contributed equally to this work.

Supplemental data for this article can be accessed here. https://doi.org/10.1080/21663831.2018.1477848

by intercalating the metal ions or introducing the metal oxide species. In addition, enhancing the active edge sites and conductivity of MoS_2 simultaneously with a single component remains a challenging task. In this respect, the development of heterostructures by coupling MoS_2 with other semiconductor materials, including graphene [6], graphitic carbon nitride [7], CoS_2 [8], MoO_3 [9], VS_2 [10], and MoO_2 [11], has been undertaken to ameliorate the poor conductivity of MoS_2 and improve the specific capacitance and long-term stability. Hunag et al. [6] developed a layered MoS_2/graphene nanocomposite via a modified L-cysteine-assisted solution phase method. The as-synthesized MoS_2/graphene nanocomposite electrode material demonstrated a maximum specific capacitance of 243 F g^{-1} at a discharge current density of 1 A g^{-1}. Ansari et al. [7] reported the use of a mechanochemically synthesized MoS_2-g-C_3N_4 heterostructure as an electrode material for supercapacitors, which delivered a higher specific capacitance of 240.85 F g^{-1} than that of pristine g-C_3N_4 (48.77 F g^{-1}) at a current density of 1 A g^{-1}. Wang et al. [8] reported the hydrothermally synthesized MoS_2/CoS_2 nanotube electrode that exhibited an excellent areal capacitance of 142.5 mF cm^{-2} at 1 mA cm^{-2} with a good cyclic stability. Zhou et al. [9] demonstrated the oxygen-incorporated MoS_2 nanosheets with rich defects that exhibited a superior specific capacitance of 145 F g^{-1} at a current density of 0.5 A g^{-1}. Nonetheless, there is still room for enhancement of the electrochemical activity of MoS_2 by coupling with other materials.

Molybdenum trioxide (MoO_3) is a class of widely used energy storage materials because of their remarkable specific theoretical capacitance, good electrochemical properties, simple, low cost and controllable preparation [12]. But, their low conductivity inhibits to use in many fields [13]. For instance, MoO_3 is regarded to be a promising candidate for energy storage and has been extensively studied in recent years [12–14]. However, MoO_3 electrode has few disadvantages including (i) sluggish faradic redox kinetics, (ii) fast degradation of cycling performance, and (iii) low volumetric capacitance, due to its poor intrinsic conductivity (10^{-5} S cm^{-1}) [14]. Several methods have been applied to increase the overall performance of MoO_3 including, coupling of MoO_3 with other materials or ion-intercalation or oxygen and nitrogen doping, etc. [11,15,16].

Zhang et al. [11] demonstrated hydrothermally synthesized Molybdenum oxide–MoS_2 electrodes that exhibited a high specific capacitance of 433.3 F g^{-1} at a scan rate of 5 mV s^{-1}. More recently, Li et al. [15] synthesized an α-MoO_3@MoS_2 heterojunction via a two-step hydrothermal method for photocatalytic applications. The MoO_3@MoS_2 heterojunction contributed to the effective separation of photoinduced carriers. Impressively, a MoS_2–MoO_3 hybrid nanostructure was developed by Yin et al. [16] and used for light-emitting diode applications. Although a lot of studies have attributed their superior supercapacitor properties of MoO_3 based hybrids to the good interfacial interaction, complete analysis of the interface is still rare until now. Therefore, we attempted to apply a MoS_2/MoO_3 heterostructure as an electrode material for a supercapacitor.

In this study, we synthesized self-assembled MoO_3 nanocrystals on three-dimensional (3D) MoS_2 nanosheets, defined as a MoS_2/MoO_3 heterostructure, which were obtained from the introduction of MoO_3 precursor oxygen bonding on MoS_2 nanosheets via a hydrothermal reaction. This kind of architecture facilitates a strategy for simultaneously enhancing the density of active edge sites and the electron transfer pathway. Moreover, the MoO_3 nanoparticles on the surface of MoS_2 layers prohibit the stacking of MoS_2 nanosheets which contribute to improved supercapacitor performance. The experimental results demonstrate that the MoS_2/MoO_3 heterostructure has a superior specific capacitance compared to that of pristine MoS_2 in an alkaline solution. Furthermore, an examination of the long-term stability shows that this heterostructure design is very stable, even after 1000 cycles. More importantly, this study illustrates a facile approach to synthesizing low-cost and highly efficient electrode materials for energy storage devices.

2. Experimental details

2.1. Synthesis of MoS_2/MoO_3

A modified procedure for synthesizing molybdenum disulfide (MoS_2) was followed as reported in our previous studies [17]. Typically, 0.14 mmol of $(NH_4)_6Mo_7O_{24}.4H_2O$ was added to 25 mL ethanol in a glass beaker. After stirring for 10 min, C_4H_4S (15 mL) was added drop by drop and immediately added HCl (2 mL) to above solution and maintained at 90°C with continuous stirring for 15 min. Then, the resultant solution was transferred into a Telfon-lined autoclave, placed inside a furnace, and maintained at 190°C for 8 h. After the nature cooling of autoclave, the products were collected using a centrifuge at 5000 rpm and washed three times with ethanol. Finally, the precipitates were heated in a vacuum oven at 110°C for 3 h.

A MoS_2/MoO_3 heterostructure was synthesized via a simple hydrothermal reaction. In a typical procedure, 20 mL of an MoS_2 (6 mg mL^{-1}) solution in ethanol containing certain amount of sodium molybdate dihydrate was isolated evenly with a magnetic stirrer for 30 min

to obtain a suspension. The resulting solution was transferred into a Teflon-lined autoclave and maintained at 190°C for 15 h. Once the autoclave naturally cooled to room temperature, the precipitates were collected via centrifugation at 7000 rpm and washed with deionized water and ethanol four times, and the as-prepared material was heated at 120°C for 16 h.

3. Results and discussion

Scheme 1 displays a schematic illustration of the formation of the MoS_2/MoO_3 heterostructure. Firstly, $Na_2MoO_4{\cdot}2H_2O$ produces Na^+ and MoO_4^{2-} ions, the MoO_4^{2-} ions react with ethanol and allows in situ nucleation and formation of MoO_3 on MoS_2.

Figure 1(a) displays the XRD patterns of the pristine MoS_2 and MoS_2/MoO_3 heterostructure. It is found that there are five diffraction peaks at $2\theta = 14.12°$, 32.91°, 39.5°, 49.41°, and 58.7°, which can be ascribed respectively to the (002), (100), (103), (105), and (110) planes of the hexagonal phase MoS_2 (JCPDS card no. 75-1539). The MoS_2/MoO_3 heterostructure possesses coexisting phases of MoO_3 and MoS_2 and additional peaks (apart from those of pristine MoS_2) at $2\theta = 12.75°$, 23.31°, 25.67°, 27.26°, 33.72°, 35.45°, 45.75°, 46.31°, 49.17°, and 55.11°, which can be attributed respectively to the (020), (110), (040), (021), (111), (041), (200), (061), (002), and (112) planes of the orthorhombic phase α-MoO_3 (JCPDS carb no. 05-0508). Interestingly, it is observed that the peak position at 13.6° related to the (002) plane shifts to the left for the MoS_2/MoO_3 sample, as compared to the peak position of the pristine MoS_2 (14.12°), indicating that the distance between the (002) planes increased, which is confirmed from the TEM image (Figure 3(e)). Apart from the (002) peak, other peaks have no apparent shifts because their corresponding interplanar spacings are too small.

Figure 1(b) shows the Raman spectrum of the MoS_2/MoO_3 heterostructure. It is observed that the Raman spectrum from 350 to 420 cm^{-1} reveals two vibration peaks at 381 and 406 cm^{-1}, corresponding respectively to the $E_{2g}{}^1$ and A_{1g} vibration modes of hexagonal MoS_2 [18]. Additional band peaks located at 284, 641, 820, and 987 cm^{-1} correspond to the α-MoO_3 crystal phase [19]. Among these, the intense broad peak at 987 cm^{-1} is ascribed to the terminal oxygen ($Mo^{6+}=O$) stretching mode along the 'a' and 'b' directions, resulting from unshared oxygen and also responsible for the nanocrystalline structure of α-MoO_3 [18,19]. The intense Raman peak at 820 cm^{-1} is assigned to the doubly coordinated oxygen (Mo_2–O) stretching mode, which results from corner-shared oxygen in common with two octahedral (i.e. alternating bond lengths of MoO_6) [19]. The Raman peaks at 284 cm^{-1} can be attributed to O–Mo–O scissoring modes of the α-MoO_3 crystal phase. Therefore, the results obtained from Raman spectroscopy analysis are in good agreement with the conclusions drawn from XRD analysis.

Figure 1(c) shows the FTIR spectra of pristine MoS_2 and the MoS_2/MoO_3 heterostructure in the range of 400–4000 cm^{-1}. The measured FTIR reflectance spectrum of pristine MoS_2 shows several significant absorption peaks positioned at 3667, 2977, 1402, 1068, 891, and 551 cm^{-1}. In the case of the MoS_2/MoO_3 heterostructure, additional peaks located at 1631, 1386, 843, 749, and 537 cm^{-1} are ascribed to the stretching and bending modes of MoO_3, which is formed by MoO_6 octahedra [19]. In addition, strong vibration peaks at 1068

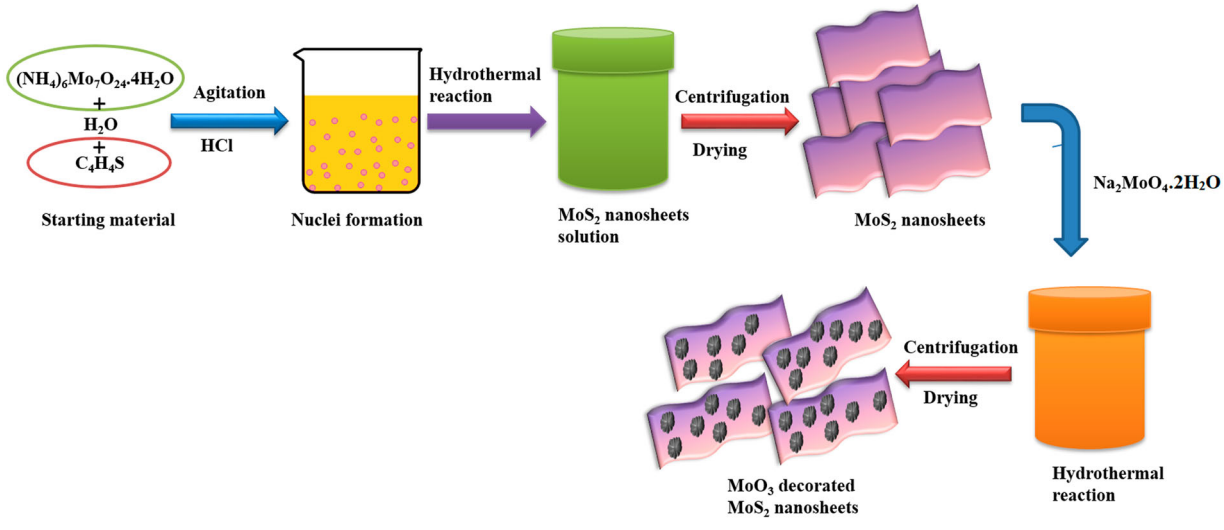

Scheme 1. Schemtic illustration of the formation of the MoS_2/MoO_3 heterostructure.

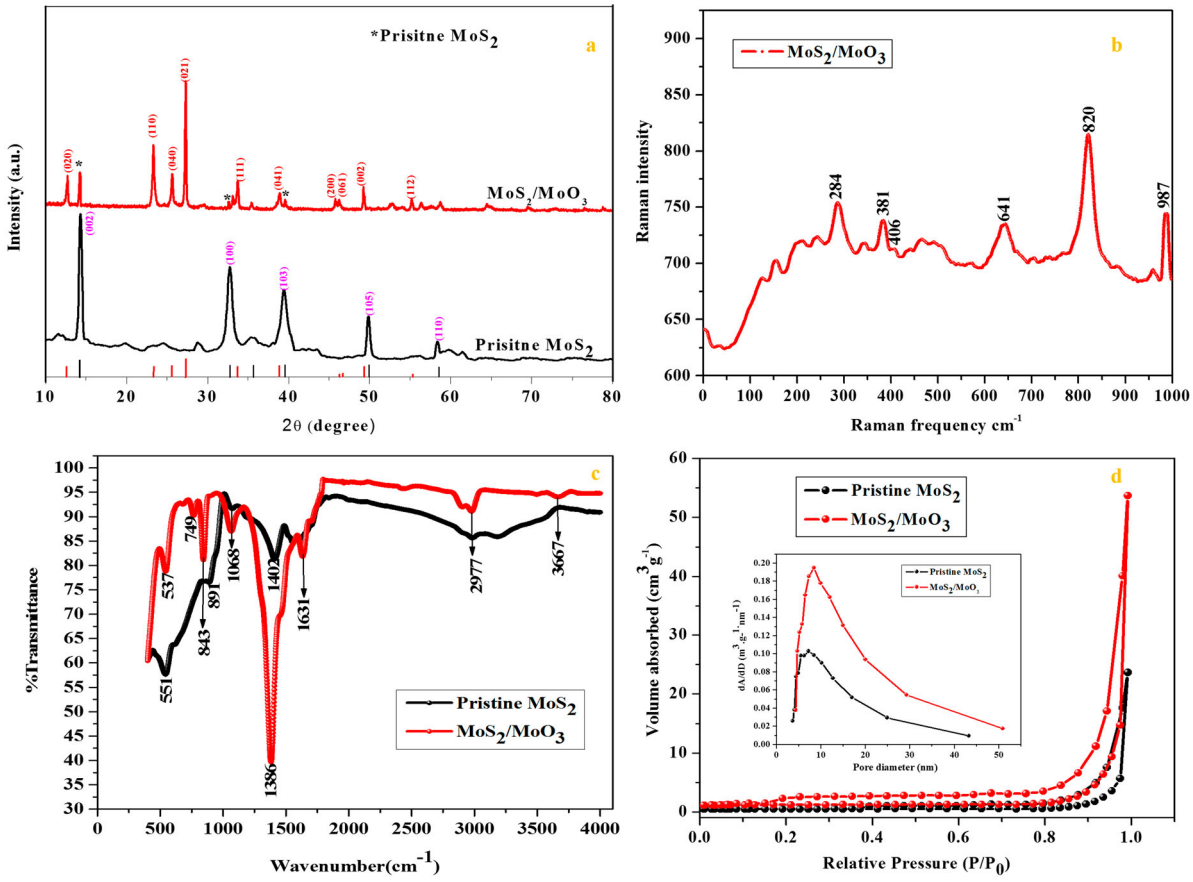

Figure 1. (a) XRD patterns of pristine MoS_2 and the MoS_2/MoO_3 heterostructure. (b) Raman spectra of the MoS_2/MoO_3 heterostructure. (c) FTIR spectra of pristine MoS_2 and the MoS_2/MoO_3 heterostructure. (d) N_2 adsorption-desorption isotherms (inset: Barrett–Joyner–Halenda (BJH) pore size distribution) data of pristine MoS_2 and the MoS_2/MoO_3 heterostructure.

and 843 cm^{-1} are assigned to the symmetric stretching mode of oxygen in the Mo–O–Mo and Mo = O stretching modes, respectively. A broad band positioned at 537 cm^{-1} corresponds to the typical vibration of the Mo_2O_2, which is formed by edge-shared MoO_6 polyhedra constructing an orthorhombic MoO_3 structure.

It is found from the BET results (Figure 1(d)) that the specific surface area of the obtained MoS_2/MoO_3 heterostructure is 56.2 m^2g^{-1}, which is higher than that of pristine MoS_2 (45.1 m^2g^{-1}). The pore size and pore volume of the MoS_2/MoO_3 heterostructure is 16.4 nm and 0.019 $cm^3\ g^{-1}$.While, the pore size and pore volume of the pristine MoS_2 is 21.3 nm and 0.012 $cm^3\ g^{-1}$. These results indicate that the obtained MoS_2/MoO_3 heterostructure comprises mesopores, which are favorable for oxidation and reduction reactions.

High-resolution XPS was carried out to determine the chemical composition and other bonding information of the MoS_2/MoO_3 heterostructure; the results are shown in Figure 2. The surveyed XPS spectra (Figure 2(a)) of pristine MoS_2 and MoS_2/MoO_3 heterostructure evidently reveals the presence of Mo and S elements and Mo, S, and O elements, respectively. Figure 2(b) shows two broad peaks positioned at 228.73 and 231.86 eV, which correspond respectively to spin orbits of Mo $3d_{5/2}$ and Mo $3d_{3/2}$ of the Mo^{4+} chemical state, and a minor peak at 225.93 eV, which is ascribed to S 2s of MoS_2. In addition, small peak at 236.1 eV corresponding to Mo^{6+} state was observed, representing the formation of oxygen bonding within the MoS_2/MoO_3 heterostructure, which is in consistent with reported literatures [20]. The formation of oxygen bonding is explained by the fact that, during hydrothermal reaction, energetic oxygen atoms of the MoO_3 contact the MoS_2 surface and the S atoms can move out of the lattice site, forming lattice vacancies. The S of MoS_2 bonding with the O of MoO_3 was also observed in the S 2p spectra. Figure 2(c) displays the XPS spectrum of S 2p. A broad peak at the binding energies of 161.78 is ascribed to S $2p_{3/2}$ and a small peak positioned at 162.85 eV is assigned to S $2p_{1/2}$ of the S^{2-} chemical state. In addition to these two peaks, a small peak at higher energy (164.5 eV) corresponds to the oxidized sulfur further prove the formation of chemical bonding in between the MoS_2 and MoO_3. Figure 2(d) displays the

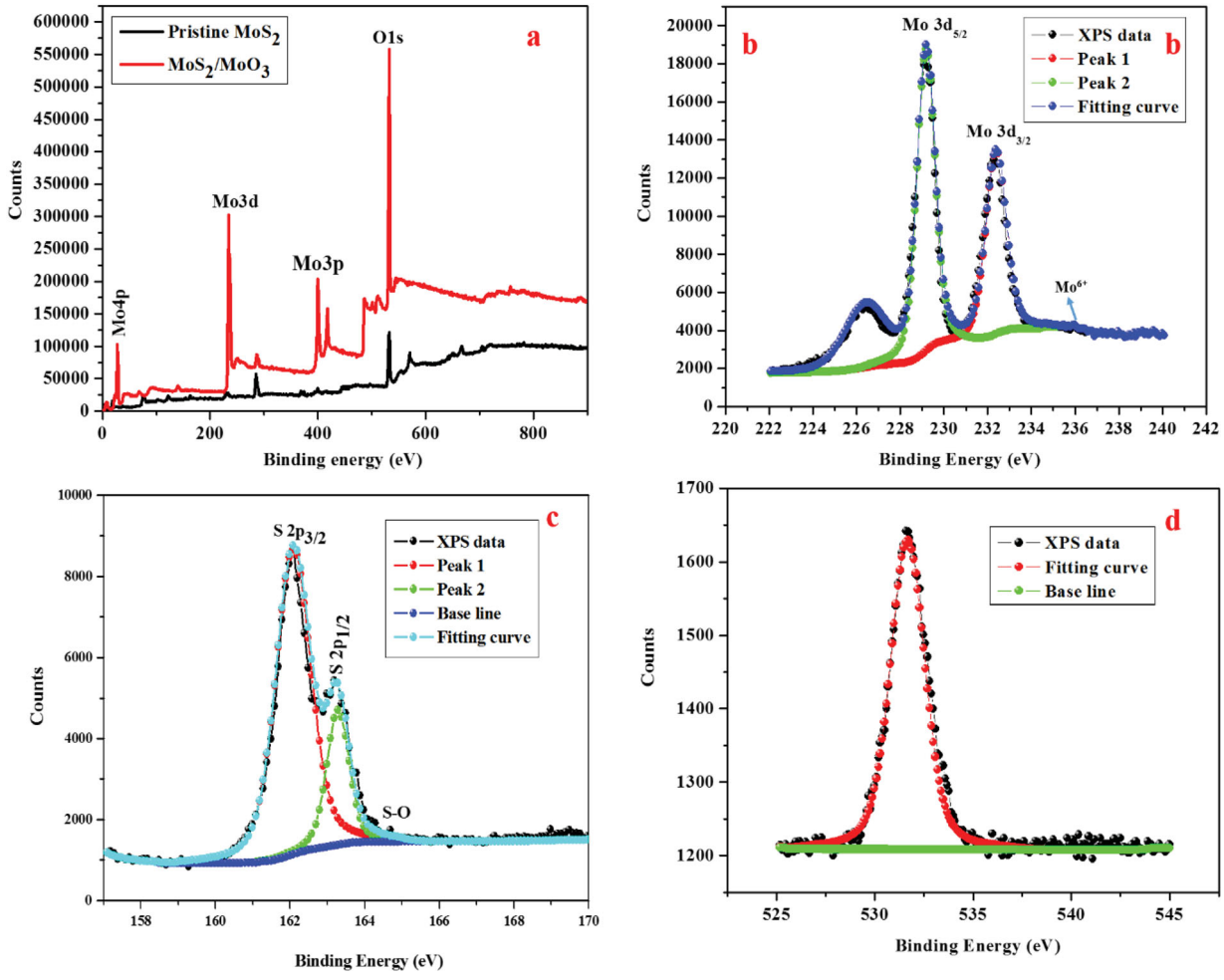

Figure 2. (a) XPS survey spectrum. XPS spectra of (b) Mo, (c) S, and (d) O of the MoS_2/MoO_3 heterostructure.

O1s peak observed at 531.52 eV, which is from the MoO_3 in the MoS_2/MoO_3 heterostructure.

Figure 3 shows representative HRTEM images of the resulting pristine MoS_2 and MoS_2/MoO_3 heterostructure samples. The 3D nanosheets possess a morphology with abundant folded edges, as can be clearly seen in Figure 3(a). From Figure 3(b), the (002) and (100) planes of the pristine MoS_2 can be clearly seen with lattice spacings of 0.63 nm and 0.27 nm. For the MoS_2/MoO_3 heterostructure (Figure 3(c,d)), it can be seen that the MoO_3 nanocrystals were uniformly decorated with 3D MoS_2 nanosheets with abundant folded edges and numerous active sites, which is favorable for enhanced supercapacitor performance. From Figure 3(e), the periodic fringe spacing of 0.37 nm agrees well with the interplanar spacing of (040) for α-MoO_3 (orthorhombic, a = 0.396 nm, b = 1.385 nm, c = 0.369 nm). In addition, lattice fringe spacing is increased (0.67 nm) for MoS_2/MoO_3 heterostructure as compared to pristine MoS_2 (0.63 nm), which is in good agreement with (002) peak shift towards smaller 2θ in XRD and suggests forming the solid solution reaction of MoO_3 in MoS_2/MoO_3. Figure 3(f) shows the selected area electron diffraction (SAED) ring pattern with a coexisting phase of the MoS_2/MoO_3 heterostructure.

Figure 4 shows the electrochemical performance of the pristine MoS_2 and the MoS_2/MoO_3 heterostructure when used as electrode materials in supercapacitors. Figure 4(a) shows the cyclic voltammetry (CV) curves for pristine MoS_2 and the MoS_2/MoO_3 heterostructure at a scan rate of 50 mVs^{-1}. The nature of CV of MoS_2 reveals that the material exhibits broad peaks which closely resemble the non-faradic reactions. While on the addition of MoO_3 to MoS_2 apart from non-faradic process the CV curves shows peaks that corresponds to faradic reaction which corresponds to pseudo capacitance behavior. In other words, the introduction of MoO_3 nanocrystals onto the MoS_2 nanosheets produces a pair of redox peaks, proving the occurrence of pseudocapacitance and reversible faradic reactions. Figure 4(b) displays the CV curves at different scan rates, ranging from 1 to 150 mVs^{-1}. As the scan rate

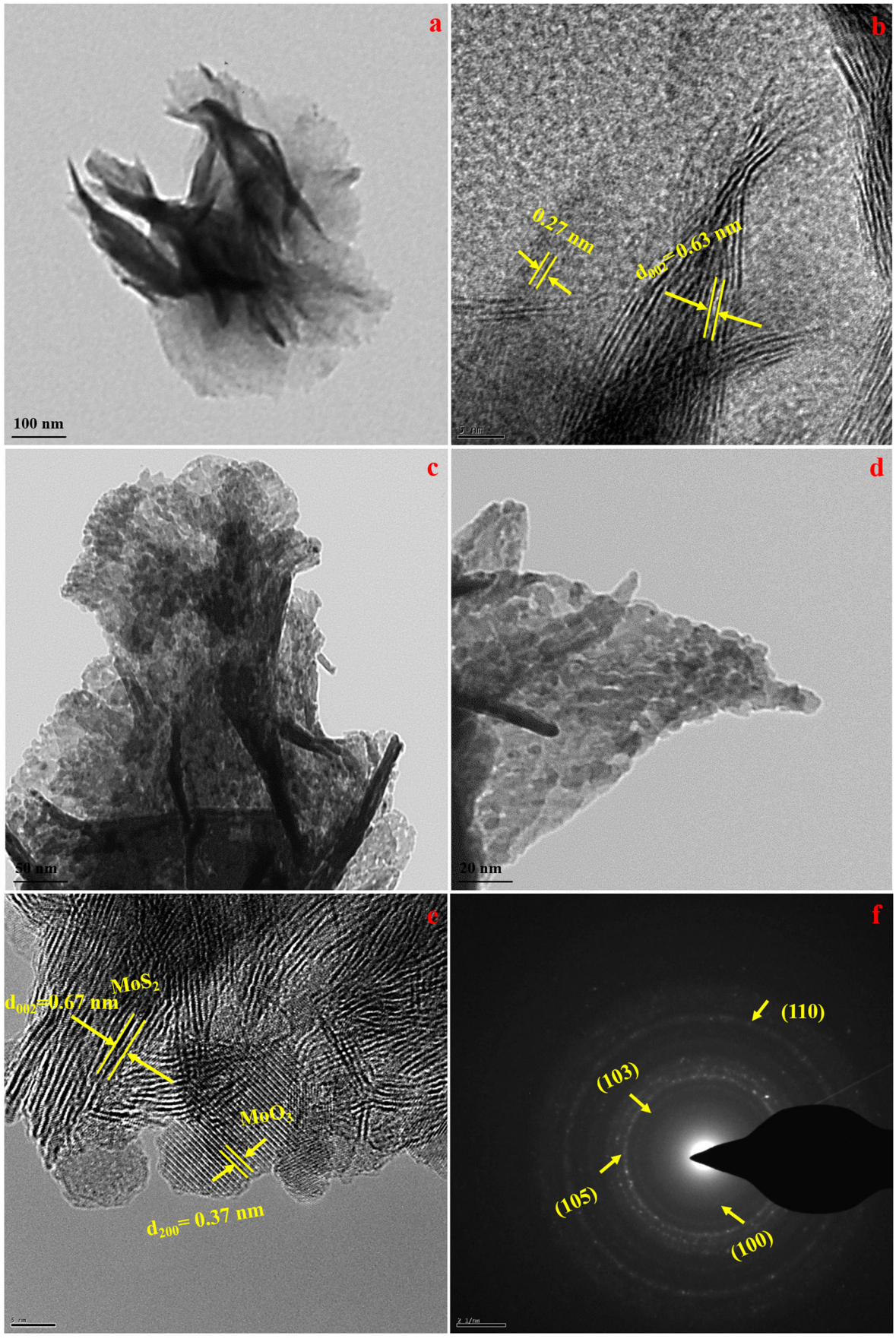

Figure 3. HRTEM images of (a,b) pristine MoS_2, (c)–(e) MoS_2/MoO_3 heterostructure, and (f) the SAED pattern of the MoS_2/MoO_3 heterostructure.

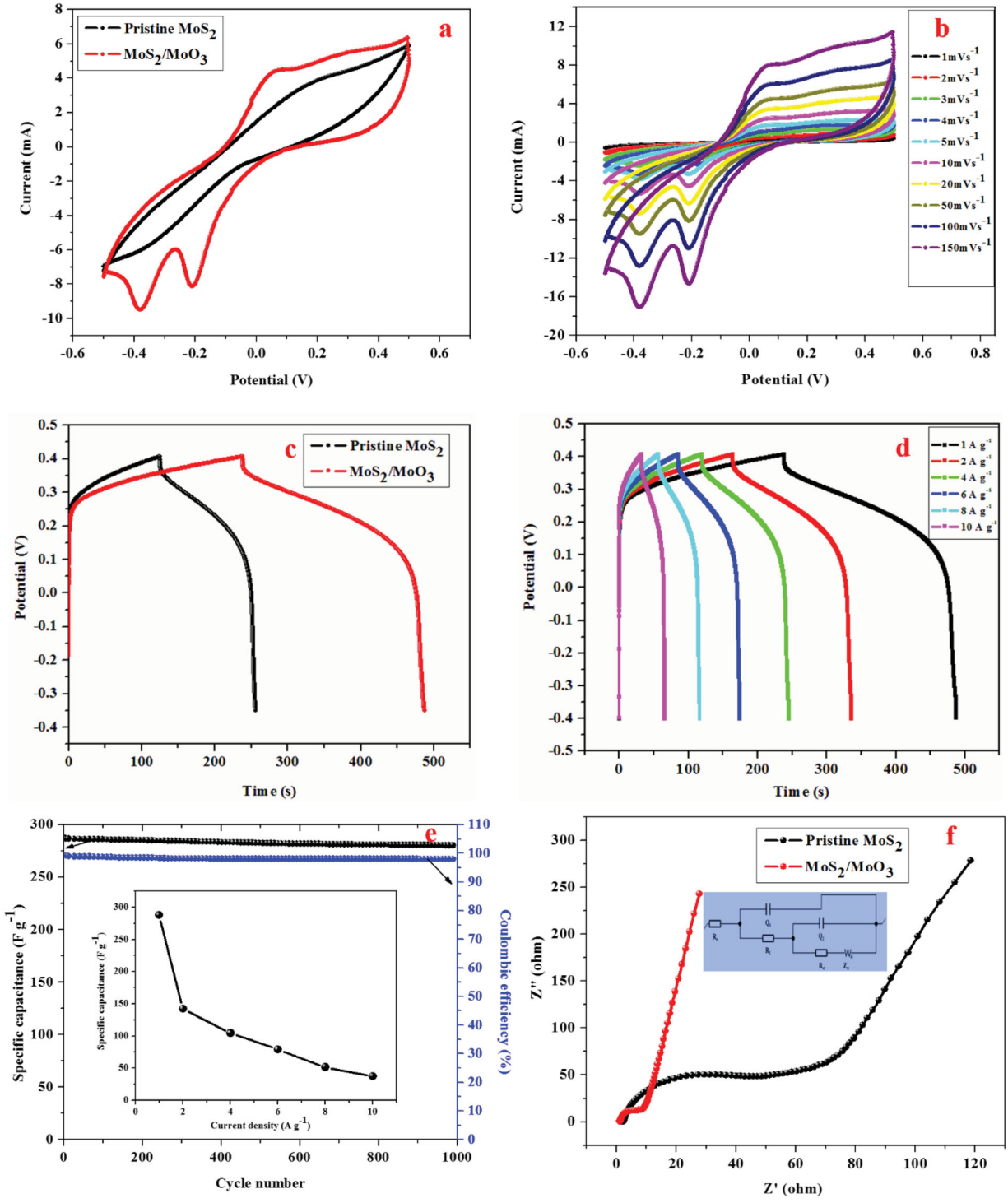

Figure 4. (a) CV curves of the pristine MoS_2 and MoS_2/MoO_3 heterostructure electrodes at a scan rate of 50 mVs^{-1}. (b) CV curves of the MoS_2/MoO_3 heterostructure at different scan rates. (c) Galvanostatic charge–discharge curves of the pristine MoS_2 and MoS_2/MoO_3 heterostructure electrodes at a constant current density of 1 A g^{-1} in 0.5-M NaOH. (d) Galvanostatic charge–discharge curves of the MoS_2/MoO_3 heterostructure at different current densities. (c) Cyclic stability and Coulombic efficiency of the MoS_2/MoO_3 heterostructure electrode for 1000 cycles at a constant current density of 1 A g^{-1}. (f) Impedance spectra in the range 100 mHz to 1 MHz of the pristine MoS_2 and MoS_2/MoO_3 heterostructure electrodes at a 0.0-V applied potential.

increases, the current response gradually increases as a result and the peak position changes. However, the shapes of the CV curves remain the same, which reflects the good electrochemical stability and scan rate performance of the MoS_2/MoO_3 heterostructure. Figure 4(c) shows the galvanostatic charge–discharge curves of the pristine

Table 1. Comparison of performance metrics for the MoS_2/MoO_3 heterostructure electrode materials with several reported electrode materials in existing literatures.

Electrode materials	Electrolyte	Current density/Scan rate ($A\,g^{-1}$)	Capacitance ($F\,g^{-1}$)	Number of cycles	Retention (%)	Ref.
MoS_2 (bulk)	1M Na_2SO_4	0.5	92	1000	~ 93.8	[25]
1T phaseMoS_2	6 M KOH	0.5	366.9	1000	~ 92.2	[26]
MoS_2/Fe_3O_4	1M H_2SO_4	1	624	2200	~ 96	[27]
MoS_2/Mn_3O_4	1M Na_2SO_4	1	119.3	2000	~ 69.3	[28]
Ni_3S_2@MoS_2	6 M KOH	0.5	1418.5	1250	~ 75.8	[29]
MoS_2/C	1M Na_2SO_4	1	411	1000	~ 93.2	[30]
$MoS_2/NiCo_2O_4$	3 M KOH	1.5	51.7	8000	~ 98.2	[31]
MoS_2/3DG	1M H_2SO_4	1	410	10000	~ 80.3	[32]
NiS_2/MoS_2	3 M KOH	0.5	108	10000	~ 100	[33]
Co_3O_4/C-MoS_2	2 M KOH	1	1076	5000	~ 64.5	[34]
$NiFe_2O_4/MoS_2$	1MKOH	1	506	3000	~ 90.7	[35]
CoS_2@MoS_2	2M KOH	1	1038	10000	~ 84.76	[36]
MoS_2/rGO	1M Na_2SO_4	1	318	5000	~ 82	[37]
$MoS_2/BiVO_4$	2 NaOH	10	166.6	200	~ 80	[38]
MoS_2/MoO_3	0.5M NaOH	1	287.7	1000	~ 97.4	This work

MoS_2 and MoS_2/MoO_3 heterostructure samples ranging at $1\,A\,g^{-1}$. In addition, Figure 4(d) displays the galvanostatic charge–discharge curves of the MoS_2/MoO_3 heterostructure sample, ranging from 1, 2, 4, 6, 8, and $10\,A\,g^{-1}$. The inset in Figure 4(e) shows the specific capacitances at the corresponding current densities and the specific capacitance is estimated like so [21,22]:

$$C = I \times \Delta t/(m \times \Delta V),$$

where I/m ($A\,g^{-1}$) is the specific current density, Δt (t) is the discharge time, and ΔV (V) is the potential window for the charge–discharge process. The MoS_2/MoO_3 heterostructure electrode exhibits specific capacitances of 287.7, 142.2, 104.2, 78.3, 51.6, and $37.4\,F\,g^{-1}$, corresponding to current densities of 1, 2, 4, 6, 8, and $10\,A\,g^{-1}$, respectively. The specific capacitance achieves a maximum of $287.7\,F\,g^{-1}$ at a low current density of $1\,A\,g^{-1}$, which is higher than that of pristine MoS_2. This enhanced performance may be ascribed to the hierarchically porous structure of the heterostructure, which may deliver shorter pathways for fast and efficient ion transport. The high capacitance may be ascribed to the pseudocapacitance caused by the central Mo atoms with valences ranging from +2 to +6 in the charge/discharge processes [23,24]. Figure 4(e) shows the cyclic stability of the MoS_2/MoO_3 heterostructure at $1\,A\,g^{-1}$, which is another critical factor for practical applications, especially at a relatively remarkable current density. From Figure 4(e), the capacitance only decreases by about 2.6% of the initial capacitance after 1000 cycles, representing a remarkable cycling life of the MoS_2/MoO_3 heterostructure. The capacitance retention upon electrochemical cycling and higher specific capacitance of the MoS_2/MoO_3 heterostructure is ascribed to (i) formation of an open structure to enhance the connection between active material and electrolyte, (ii) make full use of electrochemical active MoS_2 during the charge and discharge processes, and (iii) the improved electrical conductivity of the overall electrode [6]. The specific capacitance is $287.7\,F\,g^{-1}$ in the initial cycle and can still maintain $280.3\,F\,g^{-1}$ after 1000 cycles, giving a high capacitance retention of ~97.4%. This remarkable cyclability may be maintained because the MoO_3 is tightly attached to the MoS_2 layers, which enhances the stability of the heterostructure. Comparison of performance metrics for the MoS_2/MoO_3 heterostructure electrode materials with several reported electrode materials in existing literatures is presented in Table 1.

Table 2. Calculated EIS parameters of pristine MoS_2 and MoS_2/MoO_3.

Sample	R_s (Ω)	R_f (Ω)	Q_1 (F)	R_{ct} (Ω)	Q_2 (F)	W ($S.sec^5/cm^2$)
MoS_2	1.12	3.52	$2.7e^{-3}$	2.1	$1.45e^{-6}$	$1.03e^{-3}$
MoS_2/MoO_3	0.89	1.78	$1.59e^{-2}$	1.16	$7.86e^{-6}$	$6.2e^{-2}$

Note: R_s (Ω) denotes the electrolyte resistance attributed to the intercept of the semicircle at high-frequency range; R_f (Ω) and Q_1(F) are the SEI layer resistance and the constant phase element (CPE), respectively, equivalent to the semicircle at high-frequency range; R_{ct} (Ω) and Q_2 (F) are the charge transfer resistance and related double layer capacitor, respectively, matching to the semicircle in high-middle frequency region; and W ($S.sec^5/cm^2$) is Warburg impedance assigned to the straight line in low-frequency range related to the sodium-diffusion process.

To obtain further evidence about the improved performance of the MoS_2/MoO_3 heterostructures than pristine MoS_2 as electrodes for supercapacitor, EIS analysis was conducted in 0.5 M aqueous NaOH at 0.0 V (vs Ag/AgCl), as shown in Figure 4(f). Nyquist plots typically include a semicircle in the mid-to-high frequency region that corresponds to the charge transfer resistance (R_{ct}), and a diagonal line in the low-frequency region that corresponds to ion-diffusion behavior in the electrolyte solution and adsorption onto the electrode surface [22].The calculated EIS parameters of pristine MoS_2 and

MoS_2/MoO_3 heterostructure is listed in Table 2 (see the supplementary information file). The EIS parameter R_{ct} is estimated to be 2.1 for pristine MoS_2 and 1.16 Ω for the MoS_2/MoO_3 heterostructure. The MoS_2/MoO_3 heterostructure demonstrates a lower R_{ct} value than pristine MoS_2, which indicates that the occurrence of fast charge/discharge processes and greater electrical conductivity at the MoS_2/MoO_3 electrode–electrolyte interface. The EIS results show that the MoS_2/MoO_3 heterostructure displays more facile electrode kinetics, which is particularly useful feature for improving the performance of supercapacitance.

4. Conclusions

A simple coupling of MoS_2 with a $Na_2MoO_4{\cdot}2H_2O$ precursor via a hydrothermal chemical reaction was successfully converted to a MoS_2/MoO_3 heterostructure via oxygen bonding. This strategy involved *in situ* formation of MoO_3 nanocrystals on the surfaces of MoS_2 nanosheets, which was used as a remarkable electrode material for a supercapacitor. The MoS_2/MoO_3 heterostructure demonstrated high capacitance, excellent rate capacitance, and cyclability compared to pristine MoS_2, which may be ascribed to the unique structure of the MoS_2/MoO_3 heterostructure, comprising tiny MoO_3 nanocrystals embedded randomly in the MoS_2 nanosheets. This work offers a unique and simple approach for the formation of heterostructures that holds promise for lithium-ion batteries and photoelectrochemical cells.

Disclosure statement

No potential conflict of interest was reported by the authors.

Funding

This research was supported by the National Research Foundation of Korea (NRF) of Korea and funded by the Ministry of Science, ICT, and Future Planning (2017R1A2B1004860) and (2018R1A2B6006056). This work was supported by a NRF grant funded by the Korean government (2017R1A4A1 015581).

ORCID

S. V. Prabhakar Vattikuti http://orcid.org/0000-0002-9009-5466

References

[1] González A, Goikolea E, Barrena JA, et al. Review on supercapacitors: technologies and materials. Renew Sust Energ Rev. 2016;58:1189–1206.

[2] Zhang W, Huang K-J. A review of recent progress in molybdenum disulfide-based supercapacitors and batteries. Inorg Chem Front. 2017;4:1602–1620.

[3] Wang Y, Huang KJ, Wu X. Recent advances in transition-metal dichalcogenides based electrochemical biosensors: a review. Biosens Bioelectron. 2017;97:305–316.

[4] Acerce M., Voiry D, Chhowalla M. Metallic 1T phase MoS_2 nanosheets as supercapacitor electrode materials. Nat Nanotechnol. 2015;10:313–318.

[5] Anwar AW, Majeed A, Iqbal N, et al. Specific capacitance and cyclic stability of graphene based metal/metal oxide nanocomposites: a review. J Mater Sci Technol. 2015;31:699–707.

[6] Huang K, Wang L, Liu Y-J, et al. Layered MoS_2–graphene composites for supercapacitor applications with enhanced capacitive performance. Int J Hydrog Energy. 2013;38 (32):14027–14034.

[7] Ansari SA, Cho MH. Simple and large scale construction of MoS_2-g-C_3N_4 heterostructures using mechanochemistry for high performance electrochemical supercapacitor and visible light photocatalytic applications. Sci Rep. 2017;7:Article number: 43055.

[8] Wang L. Supercapacitor performances of the MoS_2/CoS_2 nanotube arrays in situ grown on Ti plate. J Phys Chem C. 2017;121:9089–9095.

[9] Zhou J, Fang G, Pan A, et al. Oxygen-incorporated MoS_2 nanosheets with expanded interlayers for hydrogen evolution reaction and pseudocapacitor application. ACS Appl Mater Interfaces. 2016;8:33681–33689.

[10] Samad A. $Mos_2@VS_2$ nanocomposite as a superior hybrid anode material. ACS Appl Mater Interfaces. 2017;9(35):29942–29949.

[11] Zhang T, Kong L-B, Liu M-C, et al. Design and preparation of MoO_2/MoS_2 as negative electrode materials for supercapacitors. Mater Design. 2016;112:88–96.

[12] Mai LQ, Hu B, Chen W, et al. Lithiated MoO_3 nanobelts with greatly improved performance for lithium batteries. Adv Mater. 2007;19:3712–3716.

[13] Huang L, Yao B, Sun J, et al. Highly conductive and flexible molybdenum oxide nanopaper for high volumetric supercapacitor electrode. J Mater Chem A. 2017;5:2897–2903.

[14] Yu M, Chen X, Zeng Y, et al. Dual-doped molybdenum trioxide nanowires: a bifunctional anode for fiber-shaped asymmetric supercapacitors and microbial fuel cells. Angew Chem Int Ed. 2016;55:6762–6766.

[15] Li H, Yu K, Tang Z, et al. High photocatalytic performance of a type-II a-$MoO_3@MoS_2$ heterojunction: from theory to experiment. Phys Chem Chem Phys. 2016;18:14074–14085.

[16] Yin Z, Zhang X, Cai Y, et al. Preparation of MoS_2–MoO_3 hybrid nanomaterials for light-emitting diodes. Angew Chem Int Ed. 2014;53:12560–12565.

[17] Vattikuti SVP, Byon C, Jeon S. Enhanced photocatalytic activity of ZnS nanoparticles loaded with MoS_2 nanoflakes by self-assembly approach. Physica B. 2016; 502:103–112.

[18] Qin P, Fang G, Ke W, et al. In situ growth of double-layer MoO_3/MoS_2 film from MoS_2 for hole-transport layers in organic solar cell. J Mater Chem A. 2014;2:2742–2756.

[19] Sharma RK. Synthesis and characterization of α-MoO_3 microspheres packed with nanoflakes. J Phys D Appl Phys. 2014;47:, 065305 (9pp).

[20] Kang N, Paudel HP, Leuenberger MN, et al. Photoluminescence quenching in single-layer MoS_2 via oxygen plasma treatment. J Phys Chem C. 2014;118(36)): 21258–21263.
[21] Zhai Z, Huang K-J, Wu X. Superior mixed Co–Cd selenide nanorods for high performance alkaline battery-supercapacitor hybrid energy storage. Nano Energy. 2018 (in press).
[22] Reddy PAK, Chennaiahgari M, Bodulla R, et al. Single-step hydrothermal synthesis of wrinkled graphene wrapped TiO_2 nanotubes for photocatalytic hydrogen production and supercapacitor applications. Mater Res Bullet. 2018;98:314–321.
[23] Liu X, Zhang J-Z, Huang K-J, et al. Net-like molybdenum selenide–acetylene black supported on Ni foam for high-performance supercapacitor electrodes and hydrogen evolution reaction. Chem Eng J. 2016;302:437–445.
[24] Zhang Y, He T, Liu G, et al. One-pot mass preparation of MoS_2/C aerogels for high-performance supercapacitors and lithium-ion batteries. Nanoscale. 2017;9:10059–10066.
[25] Krishnamoorthy K, Veerasubramani GK, Radhakrishnan S, et al. Supercapacitive properties of hydrothermally synthesized sphere like MoS_2 nanostructures. Mater Res Bull 2014;50:499–502.
[26] Jiang L, Zhang S, Kulinich SA, et al. Optimizing hybridization of 1T and 2H phases in MoS_2 monolayers to improve capacitances of supercapacitors. Mater Res Lett. 2015;3(4):177–183.
[27] Sarno M, Troisi A. Supercapacitors based on high surface area MoS_2 and MoS_2–Fe_3O_4 nanostructures supported on physical exfoliated graphite. J Nanosci Nanotechnol. 2017;17(6):3735–3743.
[28] Wang M, Fei H, Zhang P, et al. Hierarchically layered MoS_2/Mn_3O_4 hybrid architectures for electrochemical supercapacitors with enhanced performance. Electrochim. Acta. 2016;209:389–398.
[29] Huang L, Hou H, Liu B, et al. Ultrahigh-performance pseudocapacitor based on phase-controlled synthesis of MoS2 nanosheets decorated Ni_3S_2 hybrid structure through annealing treatment. Appl Surf Sci. 2017;425: 879–888.
[30] Zhang S, Hu R, Dai P, et al. Synthesis of rambutan-like MoS_2/mesoporous carbon spheres nanocomposites with excellent performance for supercapacitors. Appl Surf Sci. 2017;396:994–999.
[31] Wen S, Liu Y, Zhu F, et al. Hierarchical MoS_2 nanowires/$NiCo_2O_4$ nanosheets supported on Ni foam for high-performance asymmetric supercapacitors. Appl Surf Sci 2018;428:616–622.
[32] Sun T, Li Z, Liu X, et al. Facile construction of 3D graphene/MoS_2 composites as advanced electrode materials for supercapacitors. J Power Source. 2016;331:180–188.
[33] Yang X, Zhao L, Lian J, et al. Arrays of hierarchical nickel sulfides/MoS_2 nanosheets supported on carbon nanotubes backbone as advanced anode materials for asymmetric supercapacitor. J Power Source. 2017;343: 373–382.
[34] Wang B. Hierarchical mesoporous Co_3O_4/C@MoS_2 core–shell structured materials for electrochemical energy storage with high supercapacitive performance. Synth Metals. 2017;233:101–110.
[35] Zhao Y, Xu L, Yan J, et al. Facile preparation of $NiFe_2O_4$/MoS_2 composite material with synergistic effect for high performance supercapacitor. J Alloys Compd. 2017;726:608–617.
[36] Huang F, Meng R, Sui Y, et al. One-step hydrothermal synthesis of a CoS_2@MoS_2 nanocomposite for high-performance supercapacitors. J Alloys Compd. 2018;742:844–851.
[37] Kamila S, Mohanty B, Samantara AK, et al. Highly active 2D layered MoS_2-rGO hybrids for energy conversion and storage applications. Sci Rep. 2017;7:8378.
[38] Arora Y, Shah AP, Battu S, et al. Nanostructured MoS_2/$BiVO_4$ composites for energy storage applications. Sci Rep. 2017;6:36294.